OCT4-mediated inflammation induces cell reprogramming at the origin of cardiac valve development and calcification

Emily Farrar, Emilye Hiriart, Ablajan Mahmut, Bernd Jagla, David Peal, David Milan, Jonathan Butcher, Michel Puceat

DEVELOPMENTAL BIOLOGY

OCT4-mediated inflammation induces cell reprogramming at the origin of cardiac valve development and calcification

Emily J. Farrar[1]†, Emilye Hiriart[2]†, Ablajan Mahmut[1], Bernd Jagla[3], David S. Peal[4], David J. Milan[4], Jonathan T. Butcher[1]*‡, Michel Puceat[2]*‡

Cell plasticity plays a key role in embryos by maintaining the differentiation potential of progenitors. Whether postnatal somatic cells revert to an embryonic-like naïve state regaining plasticity and redifferentiate into a cell type leading to a disease remains intriguing. Using genetic lineage tracing and single-cell RNA sequencing, we reveal that Oct4 is induced by nuclear factor κB (NFκB) at embryonic day 9.5 in a subset of mouse endocardial cells originating from the anterior heart forming field at the onset of endocardial-to-mesenchymal transition. These cells acquired a chondro-osteogenic fate. OCT4 in adult valvular aortic cells leads to calcification of mouse and human valves. These calcifying cells originate from the Oct4 embryonic lineage. Genetic deletion of *Pou5f1 (Pit-Oct-Unc*, OCT4) in the endocardial cell lineage prevents aortic stenosis and calcification of *ApoE*$^{-/-}$ mouse valve. We established previously unidentified self-cell reprogramming NFκB- and OCT4-mediated inflammatory pathway triggering a dose-dependent mechanism of valve calcification.

INTRODUCTION

Embryogenesis requires coordination of many cell lineages at the origin of specific cell types to ensure a proper function of tissues and organs. Single-cell sequencing datasets for the last few years have revealed the cell heterogeneity of many tissues (*1*), but no study has assigned a specific dual tissue patterning and pathological role to the same cell type at both an embryonic stage and in disease of an adult tissue.

Cardiac valves originate early during development (E9.5 in mouse, 30 days in humans) from a delamination of endocardial cells in discrete cardiac territories [atrioventricular canal (AVC) and the outflow tract (OFT)]. Then, a subset of endocardial cells undergoes Endocardial-to-mesenchymal transition (EndMT) and mesenchymal cells proliferate within a cushion while keeping the potential to differentiate in different cell types such as smooth muscle cells, fibroblasts, or chondro-osteogenic progenitors. The cushion of mesenchymal cells will give rise to valve leaflets by a series of morphogenetic events (*2*, *3*).

Cardiac valves are affected in up to one-third of cardiac congenital diseases (*4*). Pediatric stenosis that could lead to aortic valve calcification also accounts for 6% of congenital heart defects (*5*). Furthermore, in adults, valvular diseases markedly increase with age, reaching 13% of the elderly at 75 years or older, including valve calcification (*6*).

Cell sources and the biological processes inducing calcification have been a matter of debate for many years (*7*–*9*). Bioactive calcification could arise from several scenarios: (i) valvular interstitial cell (VIC) could be activated by agents such as transforming growth factor–β into myofibroblasts (*10*), which die from apoptosis when exposed to biomechanical stresses leading to dystrophic calcification; (ii) a valvular endothelial cell (VEC) and/or (iii) a VIC could differentiate into a chondrogenic and osteoblastic cell (*11*); or (iv) a feature during embryonic valvulogenesis could become reactivated in adulthood.

To answer such a pathophysiological question and to specifically challenge the last hypothesis, we explored new avenues as to a role of a cell reprogramming process as a potential dual mediator of embryonic developmental valve chondrogenesis and adult calcification, respectively.

RESULTS

OCT4, a key transcription factor, is expressed in human calcifying aortic valve

Data from the laboratory have shown that *Pou5f1*-encoded OCT4, a so-called pluripotency factor (*12*), plays the role of a reprogramming factor by targeting chromatin modifiers to drive mesendodermal cardiogenic cell fate (*13*, *14*). OCT4 is rapidly down-regulated in any somatic cells in mouse embryo by E8.0 (*14*).

We first compared expression of OCT4 in healthy versus calcified human aortic valve leaflets obtained from 11 patients (Fig. 1). OCT4 was expressed throughout the healthy VEC as the nonfunctional cytoplasmic form, but only sparsely expressed in healthy VIC, again cytoplasmic (Fig. 1A). However, OCT4 was expressed in nuclei of subendothelial cells and in VIC close to the calcified areas, as well as in rare cells of noncalcified areas (Fig. 1B). Similarly, as recently identified (*15*), nuclear factor κB (NFκB) was also expressed in calcified valves. We thus tested whether OCT4 could also be coexpressed with NFκB. Nuclear OCT4 was coexpressed with nuclear NFκB in cells associated with early calcifying regions as marked by CD31$^+$ and SMA$^+$ cells undergoing EMT as well as in calcified areas (Fig. 1C).

[1]Nancy E. and Peter C. Meinig School of Biomedical Engineering, Cornell University, Ithaca, NY, USA. [2]INSERM U1251, Aix-Marseille University, MMG, Marseille, France. [3]Pasteur Institute, Cytometry and Biomarkers Unit of Technology and Service, C2RT, & Hub de Bioinformatique et Biostatistique–Département Biologie Computationnelle, Paris, France. [4]Cardiovascular Research Center, Cardiology Division, Massachusetts General Hospital Research Institute, Harvard Medical School, Boston, MA 02114, USA.
*Corresponding author. Email: michel.puceat@inserm.fr (M.P.); jtb47@cornell.edu (J.B.)
†These authors contributed equally to this work.
‡Co-senior authors.

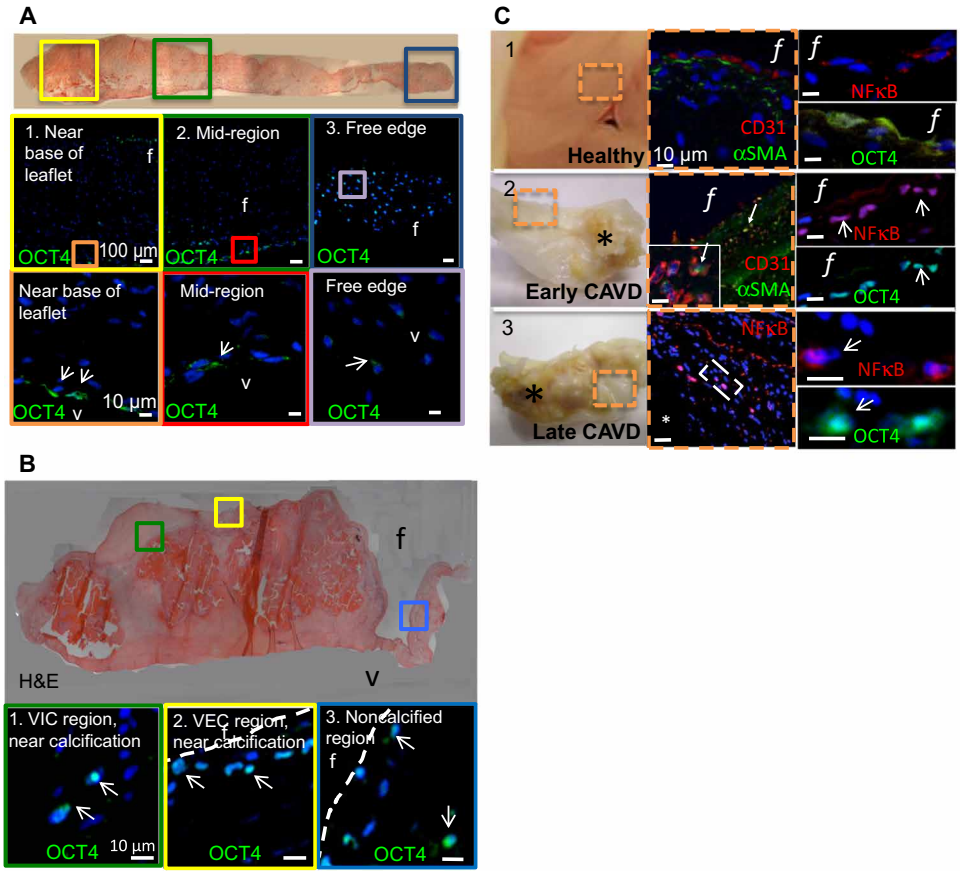

Fig. 1. OCT4 is expressed in human calcifying aortic valve. (**A**) Hematoxylin and eosin (H&E) staining of representative healthy human aortic valve leaflet. Colored boxes correspond to the magnified regions shown in lower panels (1 = base, 2 = mid, and 3 = free edge). Oct4 (green) and nuclei (blue) in each panel. Colored boxes correspond to magnified regions shown in lower panels. Scale bar, 100 (mid) or 10 μm (lower). Arrows point to OCT4$^+$ cells. (**B**) H&E staining of calcified aortic valve leaflet. OCT4 (green) and nuclei (blue) in each panel. Colored boxes correspond to magnified regions shown in lower panels. Numbers identify each region. Arrows point to OCT4$^+$ cells. Scale bar, 10 μm. (**C**) Colocalization of NFκB and OCT4 activity in aortic valve leaflets of varying levels of pathology. Orange dashed boxes in middle panels show the physiopathological status of the aortic valve regions, and the right panels show expression of NFκB and OCT4 under the corresponding status: (i) no nuclear active Oct4 or NFκB in healthy leaflets with separate CD31$^+$ endothelial cells and αSMA$^+$ VIC; (ii) early calcific aortic valvular disease (CAVD) lesions present with EndMT (coexpression of CD31 and αSMA as pointed by the arrow and highlighted in the inset) with coactive nuclear NFκB and OCT4 in transformed subendothelial cells; (iii) advanced CAVD lesions have nuclear-active NFκB and OCT4 proximal to calcified domains (*). The dashed white box highlights an area of NFκB- and OCT4-coexpressing cells. Representative images from $N = 11$ valves; f, fibrosa; v, ventricularis. Photo credit: Emily Farrar (Cornell University).

OCT4 mediates NFκb-induced cell reprogramming, endothelial-to-mesenchymal transition (EndMT) of aortic valvular cells

To better understand the pathophysiological relevance of these OCT4$^+$ cells, we first used an established in vitro model system. As human valvular cells acquired from heart donors regularly exhibit evidence of spontaneous EndMT (*16*), we chose the closest well-characterized cell source and method, 3D cultured porcine aortic VEC and VIC (*17*).

We first asked whether NFκB could turn on OCT4 at the adult pathological state as this transcription factor was previously reported to induce EndMT (*18*, *19*), and it is a well-known trigger of inflammation possibly at the origin of calcification. NFκB could work upstream of Oct4. Using anti-NFκB chromatin immunoprecipitation (ChIP) sequencing data from tumor necrosis factor–α (TNFα) stimulated human immune cells from the GEO dataset (http://genome.ucsc.edu/cgi-bin/hgTrackUi?db=hg19&g=wgEncodeSydhTfbs), we found that *Pou5f1* featured some NFκB sites in a regulatory region of the gene (Fig. 2A) occupied by the H3K27ac epigenetic mark, an index of active gene transcription (Encode data; Fig. 2A, inset; http://genome.ucsc.edu/cgi-bin/hgTrackUi?db=hg19&g=wgEncodeSydhTfbs). To validate this piece of data in valvular cells, we performed anti–NFκB(p65)–ChIP–polymerase chain reaction (PCR) of DNA-bound chromatin from human VIC transfected with *p65/relA* DNA. We found that the transcription factor occupies the *Pou5f1* proximal enhancer in valvular cells specifically expressing NFκB (Fig. 2B).

A transcriptomic profile of NFκB-stimulated (p65/RelA-transfected) VEC revealed up-regulation of EndMT-related genes accompanied by stem cell pluripotency genes such as *Pou5f1*, *Nanog*, and *Klf4* expression as well as chondro-osteogenic genes (Fig. 2C and data files S1 and S2). Together, this suggests that the inflammatory signal triggers an OCT4-mediated cell reprogramming at the origin of chondro-osteogenic cells.

To test whether NFκB was sufficient to reprogram VEC via OCT4, we transfected VEC with *p65/RelA* (NFκB) or the inhibitory *Ikk*B. We found that NFκB activation induced *Pou5f1* (*Oct4*)

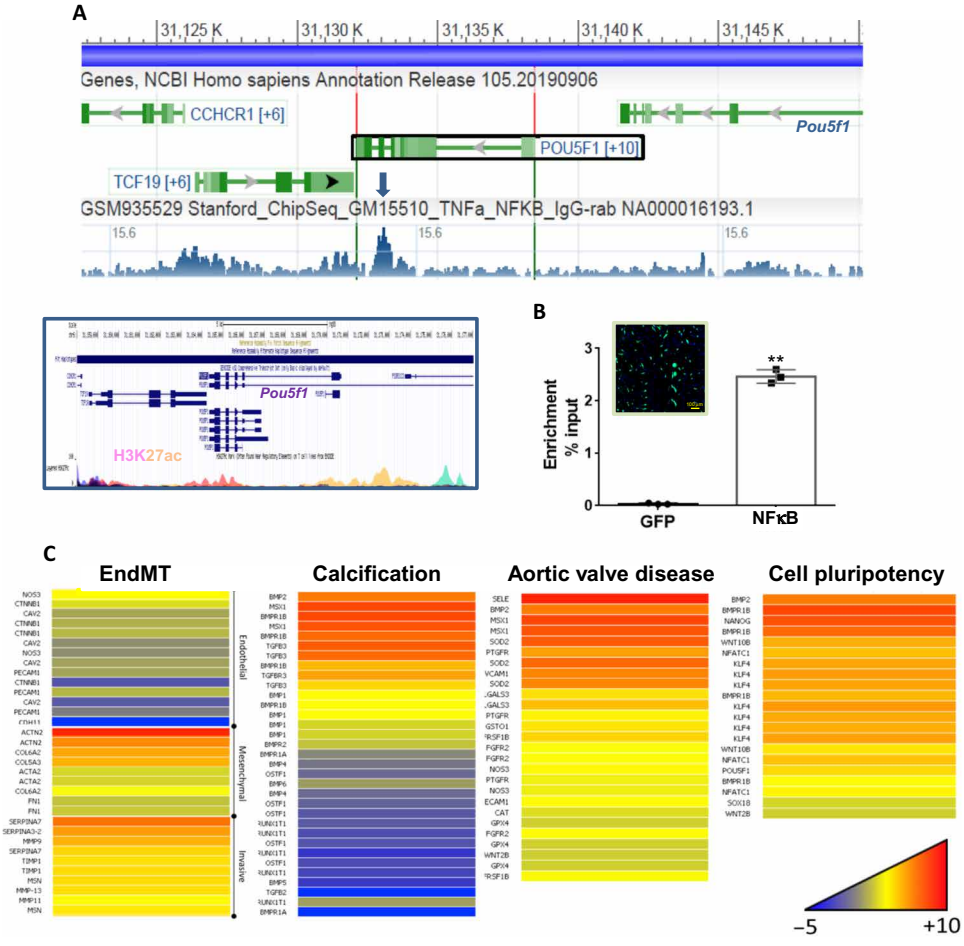

Fig. 2. NFκB turns on OCT4, pluripotency, and osteo-chondrogenic genes in valvular cells. (**A**) NFκB binding sites (Stanford_ChipSeq_GM15510_TNFa_NFKB_IgG-rab) and inset below, H3K27ac enrichment in the *POU5F1* genomic region of human cells (Encode data, http://genome.ucsc.edu/cgi-bin/hgTrackUi?db=hg19&g=wgEncodeSydhTfbs). The arrow points to a binding site within the POU5F1 gene. (**B**) Anti-p65 ChIP and PCR of *Pou5f1* proximal CR2 enhancer from chromatin extracted from GFP- or RelA/p65-transfected human VICs ($n = 3$ experiments; $^{**}P \leq 0{,}001$, Student's t test); inset: GFP-transfected cells were imaged 24 hours later to check transfection efficiency just before preparation of chromatin. (**C**) VEC^{+} NFκB transcriptional profiling. mRNA-seq of VEC transfected with RelA/p65 subunit of NFκB against vehicle. Significantly changed genes represented via color scale: blue, down-regulated; red, up-regulated. See tables for list of changes genes and their fold changes. Data are the mean fold change of $n = 3$ replicates. **Significantly different, $P \leq 0.001$, Student's t test.

expression, while its inhibition did not affect *Oct4* expression (Fig. 3A). *Oct4* transcription occurred also rapidly (<30 min) upon TNFα-induced NFκB. *Oct4* gene expression remained sustained over at least 4 hours (Fig. 3B). Transfection with *IkkB* substantially prevented TNFα induction of *Oct4*. Further, we determined that *Snai1* transcription (required for EndMT) occurred later than *Oct4* (2+ hours) (Fig. 3C). The inflammatory scenario also occurred ex vivo. Stimulation of mouse aortic valve leaflets cultured as explants in the presence of TNFα and/or osteogenic growth medium (OGM) induced Oct4 expression (fig. S1A).

Next, we investigated whether NFκB activation–induced EndMT in VEC is coordinated by OCT4. Three-dimensional (3D) cultured VEC transfected with *p65/RelA* underwent EndMT over 4 days (Fig. 3D) as previously described (*20*). Transformed cells invaded the underlying collagen matrix and can thereby be separated from VEC that resist transformation. *Oct4* expression segregated almost exclusively to the transformed population (Fig. 3, D and E). Furthermore, after 4 days of culture, the transformed cells retained elevated *Oct4* (*Pou5f1*) with almost no expression of *Snai1* or *VE-Cadherin*, supporting complete transformation to a mesenchymal progenitor phenotype, while the nontransformed cells that remained on the surface retained endothelial phenotype without Oct4 despite the presence of activation via NFκB/*RelA* transfection and TNFα (30 ng/ml; Fig. 3, E and F).

OCT4 mediates inflammatory cytokine-induced EndMT and calcification of valvular cells

We then tested whether *Oct4* was induced in VEC and/or VIC ex vivo and in vitro by proinflammatory conditions previously shown to induce calcification (*15*, *21*). Aortic mouse leaflet in culture in the presence of TNFα featured Oct4 expression (fig. S1A). Fourteen days of 3D culture in OGM + TNFα (30 ng/ml) induced *Oct4* mRNA expression in both VIC and VEC, with greater induction when stimulated in 3D coculture (fig. S1B).

We next tested whether OCT4 activation influences osteogenic differentiation and matrix calcification in VECs and VICs. VEC

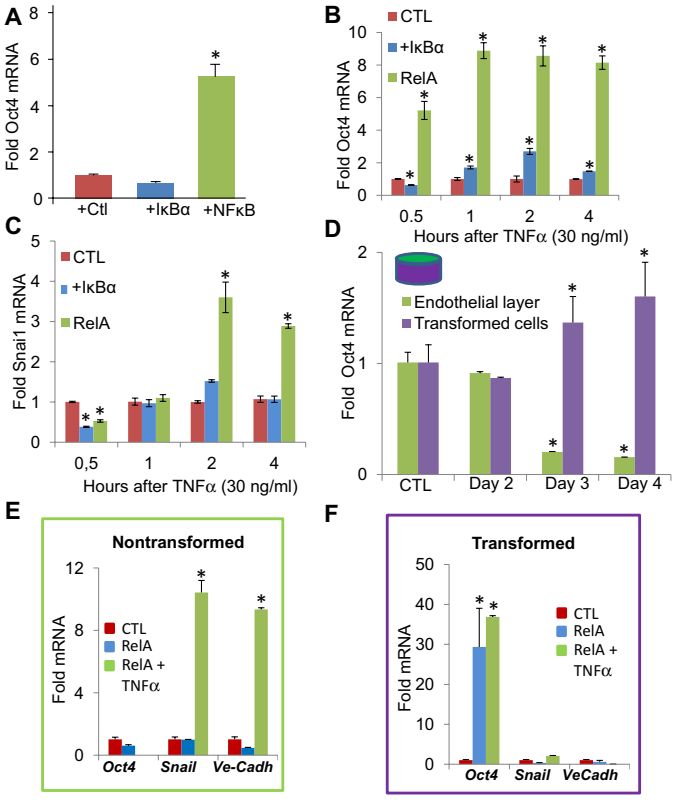

Fig. 3. Inflammatory reprogramming of valve cells via Oct4 drives disease cell phenotypes. (**A** to **C**) Transcriptional dynamics of VEC transfected with p65/RelA (+Nfkb) versus inhibition of NFκB via IκBα transfection. VEC with activated Nfkb rapidly transcribe Oct4 within 30 min upon stimulation with TNFα, which precedes snail transcription. Both are prevented with IκBα transfection. (**D** to **F**) Temporal dynamics of gene expression and cellular response of VEC to inflammatory activation. VECs that undergo EndMT retain elevated *Oct4* transcripts, whereas VECs that remain untransformed down-regulate *Oct4*. The nontransformed VECs express both VE-Cad and Snail transcripts only when NFκB is activated, whereas VECs that have undergone EndMT retain high levels of *Oct4* and have down-regulated both *Snail* and *VE-Cadherin* (*VEcadh*). *$P < 0.05$ in (A) to (F) (ANOVA). Data and images are representative of $n > 3$ independent experiments. CTRL indicates that an empty vector was used.

(fig. S2A) and VIC (fig. S2C) transfected with *Oct4 (Pou5f1)* up-regulated three times the transcript. Cotransfection of the *Pou5f1* complementary DNA (cDNA) antisense together with the sense cDNA in VIC prevented increase in expression of *Oct4* (fig. S2C). The protein OCT4 was also increased (fig. S2, B and D) in *Pou5f1* cDNA–transfected VEC (fig. S2, B and D), and this was sustained up to 14 days (fig. S2F). *Pou5f1* cDNA anti-sense expressed in VEC impaired after 14 days cell viability as suggested by DNA breakdown (fig. S2G).

VIC transfected with *Oct4* to induce nuclear activity (fig. S3, A to C) markedly up-regulated pro-osteogenic mRNA for osteocalcin (*OCN*) and protein deposition compared to empty vector control (fig. S3A). OCT4 activation induced the osteogenic gene *OCN* and protein (fig. S3A). Furthermore, with proinflammatory OGM supplementation, *OCN* mRNA and protein expression was increased synergistically with *Oct4* transfection. Cultures were further assessed for calcium deposition via Alizarin Red assay (*21*). OGM-induced calcium deposition by VIC was further increased with *Oct4* transfection (fig. S3B). Oct4 antisense transfection (Oct4AS) significantly reduced calcium deposition in OGM-cultured VIC despite the fact that *OCN* mRNA was up.

Last, we assessed whether OCT4 influences osteogenic differentiation of VEC. Oct4 synergistically increased the osteogenic effect of OGM on *Runx2* and *OCN* mRNA expression (fig. S4AB), as well as on calcium deposition (fig. S4C). We observed calcium deposition from 14-day 3D cultured VEC treated with OGM and transfected with Oct4 similar to 3D cultured VEC transfected with *RelA/NFκB* (fig. S4D). In contrast, *Oct4AS* transfection prevented calcification in both conditions. Together, these results demonstrate the importance of Oct4 activity in osteogenic and calcific differentiation of valve cells.

Genomic targets of OCT4 in valvular cells

To identify in a genome-wide manner the specific genomic targets of the transcription factor OCT4 in valve cells, *Oct4* was expressed in VIC to a limited extent (i.e., 2.7-fold increase; inset, Fig. 4) to mimic the pathological scenario as shown in VEC (fig. S2). We then performed anti-OCT4 ChIP sequencing in *Pou5f1*-transfected VIC. Peak calling identified 1445 peaks enriched over input (data file S3). Among top targets, OCT4 was bound to regulatory regions of genes that are known to be involved in EMT/EndMT and osteoblast cell fate. Enriched peaks were found in genomic regulatory regions of *SOX9*, *RUNX1*, *CDH11* (*OR OB-CDH*), *OSTF1*, *SPARC*, *MSX2*, and *SP7* (*OSTERIX*) (Fig. 4A). Furthermore, OCT4 still occupied the EMT genes (*TWIST1,2*), genomic regulatory regions, and stem cell pluripotency genes, *SOX2* and *NANOG* (Fig. 4B), an index of cell reprogramming. A few genomic regulatory regions of gene targets of Oct4 in ChiP-seq [*RUNX1*, *RUNX2*, *RUNX1T1*, *MSX2*, *HAPLN1*, *SP7* and (*OSTERIX*)] were validated by ChIP-Q PCR (Fig. 4B). None of myocardial genes such as *NKX2.5*-, *MEF2C*-, and *MYOSINS*-encoding genes were targeted by Oct4 (data file S3). This suggests that OCT4 acts as an epigenetic modifier and opens chromatin at specific osteogenic gene loci to reprogram and convert valvular cells into chondro-osteogenic cells.

Embryonic origin and phenotype of Oct4$^+$ cells

Next, we wondered whether the OCT4$^+$ cells in calcified valves could originate from reactivation of resident early valvular progenitor cells primed during embryogenesis. To test a potential embryonic origin of these cells, we used a genetic lineage tracing approach. Pou5f1^{CreErt2} mice were bred with the reporter Rosa26^{tdTomato} mice. Tamoxifen was given by a gavage to pregnant mice at E7.5 and E8.5 stages of gestation to trigger recombinase enzymatic activity during a short postgastrulation time window (E8.0 to E9.0). Embryos were collected at E10.5. Tomato$^+$ cells were observed both in the OFT and adjacent anterior heart forming field, i.e., the pharyngeal endoderm, as well as in the AVC, specifically in the endocardium but not in the myocardial cells (Fig. 5, A and B). At neonatal stage (P0), tomato$^+$ cells were specifically and only observed in the valves (both mitral and aortic) in a subset of cells (Fig. 5C). Furthermore, endocardial cells that delaminated from the myocardium and early VIC retained expression of Oct4 as shown by immunostaining of tomato$^+$ cells in the AVC of Tie2^{cre}/Rosa26^{tdTomato} E9.5 offspring (Fig. 5D).

To confirm endocardial identity of OCT4$^+$ cells, we further bred Tie2^{cre} with Rosa26^{tdTomato} mice and collected the embryos at E9.5 (18 to 20 somites). Both OFT and AVC were dissected out, and cells

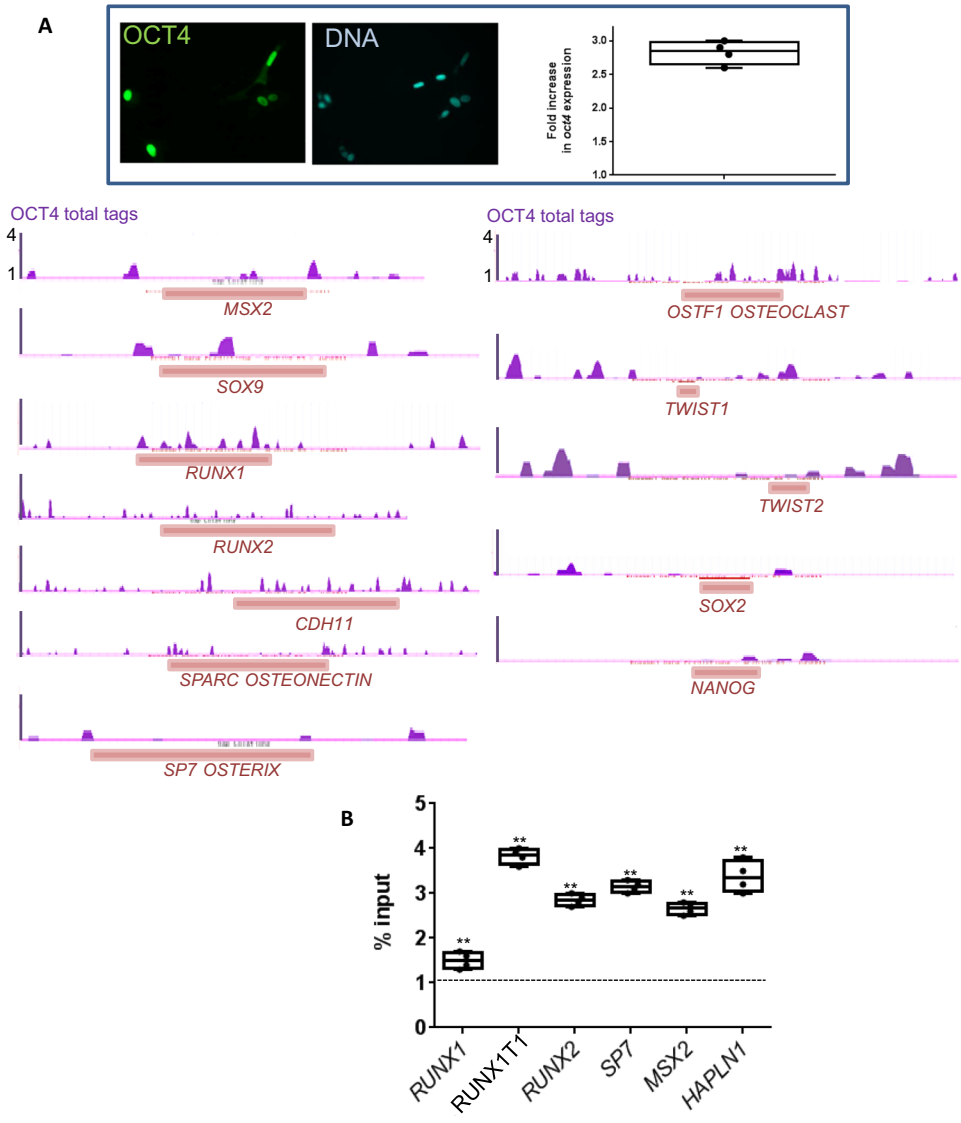

Fig. 4. OCT4 binds genomic regulatory regions of osteogenic genes in valvular cells. (**A**) Anti-OCT4 ChIP sequencing in VIC. VICs were electroporated with *Pou5f1* cDNA to express OCT4 and used in ChIP sequencing. To determine the enrichment peaks with narrow binding over input, dataset was uniformly processed using the MACS2 with defaults parameters. See tables for list of peaks. The pink boxes below the peaks show the location of the genes. Inset: OCT4 immunostaining of a few transfected cells replated before chromatin preparation and Q-PCR of *Pou5f1* (*Oct4*) of transfected cells ($n = 4$ experiments). (**B**) ChIP-PCR of osteogenic genes from PAVIC expressing OCT4 as in (A). Experiments were performed as two biological replicates and in duplicate immunoprecipitation experiments. $^{**}P \leq 0.001$, Student's *t* test (enrichment *versus* input)

were enzymatically dissociated. Single-cell PCR confirmed expression of *Pou5f1* in a restricted cell population (10 to 20%) among both OFT and AVC cells. Expression of the gene reached the same level as in mouse embryonic stem (ES) cells (Fig. 6A). We further used a single-cell RNA sequencing (RNA-seq) approach. Pou5f1^{CreErt2} mice were bred with Rosa26^{tdTomato}. The recombinase was induced by tamoxifen gavage of the pregnant female at E7.5 (Cre induced at E8.0) and E8.5 (induction at E9.0). Sixty E9.5 embryos from seven litters were collected. AVC and OFT were dissected out, and cells were dissociated from both OFT and AVC cells. Of 3500 fluorescence-activated cell sorting (FACS)–sorted cells collected from 60 embryonic AVC and OFT, 1044 tomato$^+$ cells were sequenced and analyzed covering 27,399 genes and expressing an average of 2525 genes per cell. Their transcriptomic profile was visualized by the heatmap (Fig. 6B) using a dimensionality reduction uniform manifold approximation and projection method (UMAP) (Fig. 6C) graph. Cluster identity was assigned according to a pattern of gene markers as seen in the heatmap (Fig. 6B) and the UMAP (Fig. 6C). This approach revealed first a cell cluster of endocardial cells expressing *cdh5*, *egfl7*, *emnc*, *eng*, and *pecam1* (Fig. 6B, cluster 1) and a cluster (cluster 4) of epithelial/endothelial *Epcam*$^+$, *Cldn4*$^+$, *Cldn7*$^+$, and *Pecam1* cells expressing *FGF8*, *Crabp1*, *Efna1*, and *Nkx2-5*, as well as for a subset of cells, *Epha1*, *Epha2*, *Isl1*, *Pax9*, and *Ezh2*, all markers of anterior pharyngeal endoderm (*22*). Four other cell clusters (clusters 0, 2, 3, and 5) were hybrid cells (i.e., expressing both endothelial and mesenchymal genes) competent to undergo EndMT. They further acquired a migratory potential as shown by expression of *Sepw1* and *lgals1* (*23*). Clusters 0 and 5 included endothelial/pharyngeal

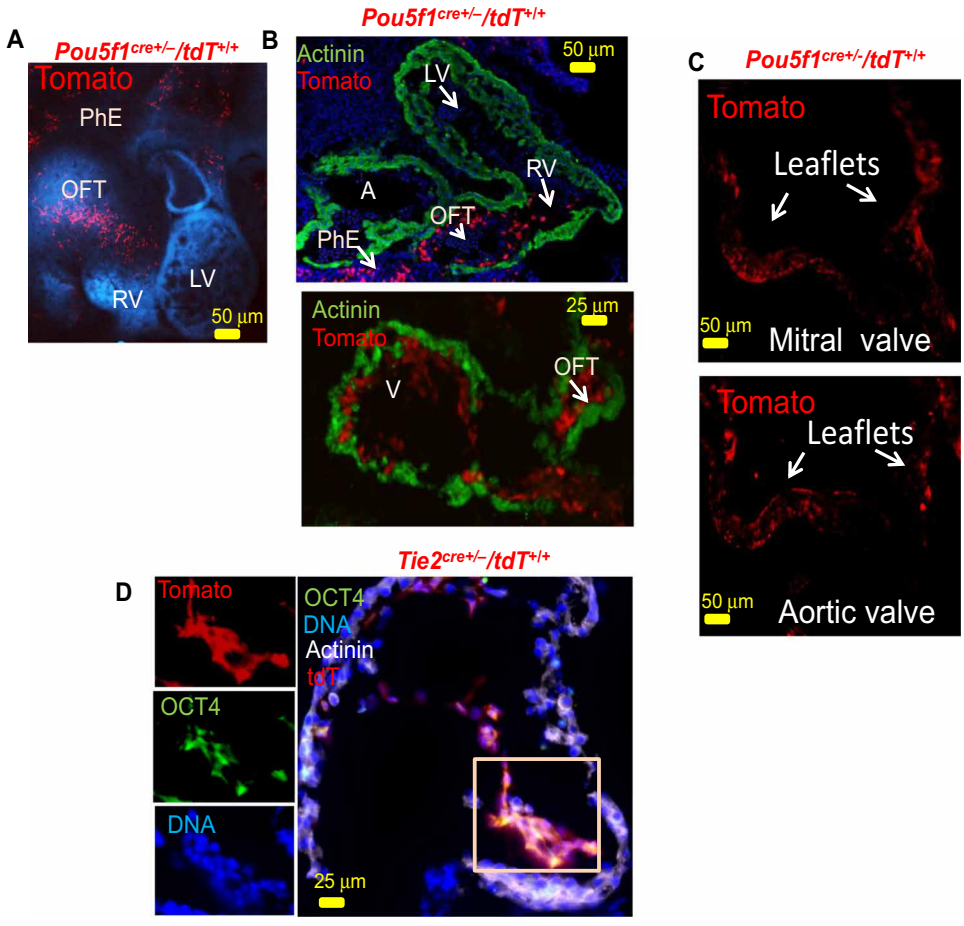

Fig. 5. Lineage tracing of Oct4$^+$ cells in mouse embryos. (**A** and **B**) *Pou5f1*^{CreERT2} mice were bred with ROSA26^{tdTomato} reporter mice. Female were gavaged with tamoxifen/progesterone at E.7.5 and E8.5 to induce the Cre at E8.0 and E9.0. (A) Embryos were collected at E10.5 and transparized, and 3D images were acquired in confocal microcopy with a long distance 10× objective or (B) frozen and cut in 10-µm sections. Sections stained with an anti-sarcomeric actinin antibody were imaged in confocal microscopy together with the tomato. LV and RV, left and right ventricles; A, atrium; PhE, pharyngeal endoderm. (**C**) *Tie2*^{Cre} mice were bred with *ROSA26*^{tdTomato} reporter mice, and embryos were collected at E9.5. Embryo sections were stained with anti-OCT4 and anti-sarcomeric actinin antibodies. The top image shows the AVC, and the three panels at the bottom a magnification of the cushion area (white square) and separate channels. (**D**) Neonatal hearts of *Pou5f1*^{CreERT2} /*ROSA26*^{tdTomato} neonates were collected and cut in 10-µm sections. Sections including mitral or aortic valve were imaged in confocal microscopy together with the tomato. Images are representative of at least six embryos and six neonatal hearts.

endodermal cells and early *Itgb1*$^+$ hybrid cells, expressing both endothelial and mesenchymal (*tagln2*) cell markers (*24*). *Twist*, *Snai1*, and target genes *Prrx1* and *Prrx2* were expressed in cluster 3 together with low pecam1 and egfl7. This cluster thus included late hybrid cells. Cluster 2 included chondro-osteoblastic progenitor cells with high expression of *Col2a1*, *Acta2*, and *Tagln* and a full loss of endothelial genes (Fig. 6B). We also used an inference trajectory approach. This bioinformatic approach revealed that both endocardial cells and pharyngeal endodermal cells from the Oct4 lineage underwent EMT at a crossroad to give rise to chondro-osteogeneic cells or late hybrid cells (Fig. 6D).

The cells during their progression toward osteo-chondrogenic progenitors, as shown by expression of *Idh3a*, wnt pathway genes (*Tcf4* and *Lef1*), *Smad1*, *Elk3*, *Dlat*, *Ppargc1a*, and the estrogen receptor *ERRα in cluster 2* (*25*) (fig. S5A), expressed the pluripotency markers *Nanog* and *Sox2* together with EMT genes *Twist* and *Snai1*, as well as known OCT4 targets, *Sall4* and *Chtop* (chromatin target of PRMT1), and the polycomb genes *Ezh2* and *Bmi1* (*26*) (fig. S5B).

Single-cell analysis of E9.5 OFT and AVC from the Tie2 lineage (Tie2^{cre}/Rosa26^{tdtomato}) further showed that *Oct4* (*Pou5f1*) was expressed in most of the clusters including cells reflecting the different stages of EMT (fig. S5C).

We repeated the single-cell RNA-seq approach from Pou^{CreERT2}/Rosa26^{tdTomato} embryos (Cre induced at E8.0) collected at E10.5. The OFT and AVC cardiac regions were dissected out together with the anterior pharyngeal region nearby the OFT. Tomato$^+$ cells were sorted by FACS and sequenced. Both the UMAP and the heatmap showed the presence of *Pecam1*$^+$, *Eng*$^+$, *Emcn*$^+$, and *Cdh5*$^+$ endocardial cells (cluster 5), as well as of pharyngeal endodermal cells expressing *Crabp1*$^+$, *FGF8*$^+$, *Sox9*$^+$, *Hes1*$^+$, *Bmp4*$^+$, *Hoxb1*$^+$, *Pax9*$^+$, *Tbx1*$^+$, *Hes1*, and *Shh*$^+$ (clusters 1 and 2). These cells were found at different stages of EMT from early hybrid *Twist1*$^+$ *Prrx1*$^+$, *Zeb1*$^+$, *Snai1*$^+$, and *Msx1*$^+$ cells (clusters 0 and 2) to *Cdh11*$^+$, *col2a1*$^+$, *Tagln*$^+$, and *Acta2*$^+$ mesenchymal and osteochondrogenic cells (clusters 6 and 4). Minor *Itgb1*$^+$ and *Acta2*$^+$ or *Acta2*$^-$ cell populations reflected different stages of EMT of still endodermal/endocardial cells (clusters 7 and 8).

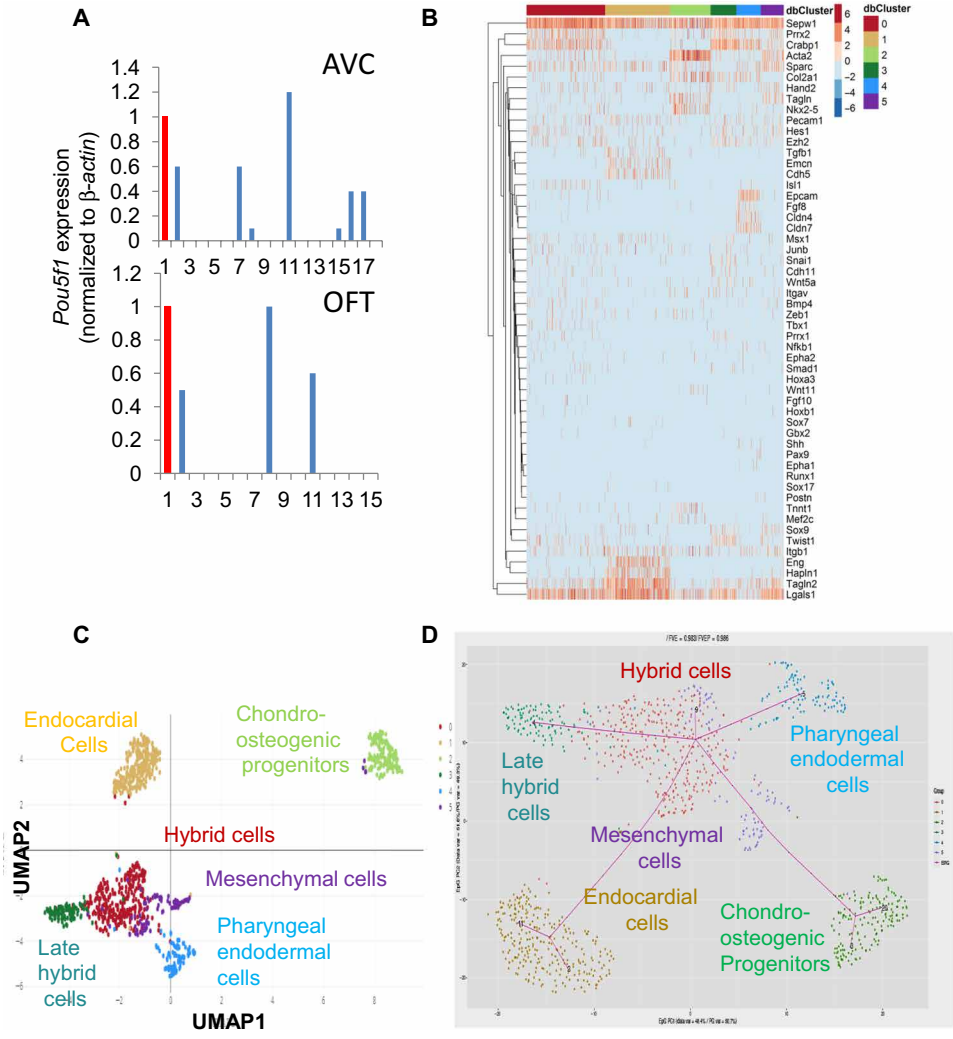

Fig. 6. Single-cell analysis of Oct4 cell lineage. (**A**) Single-cell PCR of Tomato$^+$ cells collected from the AVC or OFT of E9.5 *Pou5f1*^{CreERT2} *ROSA26*^{tdTomato} embryos from six litters. The red bar indicates expression of Pou5f1 in a single mouse ES cell that was used as a reference (set to 1). (**B**) Heatmap of single-cell RNA-seq of AVC and OFT *Pou5f1*^{CreERT2} *ROSA26*^{tdTomato} embryos. (**C**) UMAP plot showing different clusters or cell types within the cell population. (**D**) Inference trajectory (using Elpigraph) of AVC and OFT *Pou5f1*^{CreERT2} *ROSA26*^{tdTomato} cells revealing their cell fate.

It should be noted that pharyngeal endodermal cell genes were also observed in AVC and OFT tomato$^+$ cells from the Tie2^{cre}/Rosa26^{tdtomato} single-cell RNA-seq dataset (fig. S5C).

Role of OCT4$^+$ cells in embryonic valvular progenitor cells

To further investigate the valve developmental function of endocardial Oct4$^+$ cells, the reprogramming factor was overexpressed or inhibited in endocardial cells at the onset of EndMT by injecting into the AVC or OFT of E9.5 and E10.5 embryos, respectively, a cell transfection mix of lipofectamine and a plasmid harboring either a *Pou5f1* cDNA, a *Pou5f1* antisense cDNA, and/or *Ikk*B or *RelA/p65* cDNA, or an empty pcDNA vector (control mock). After 3 hours of embryo culture in the presence of 2,3-butanedione monoxime (BDM) to prevent a leakage of the DNA following heart contraction, whole OFT or AVC was dissected out and set on collagen gels to monitor the EndMT potential of these cells for the next 48 hours.

Figure 7A shows that *Pou5f1*-overexpressing cells shown by strong OCT4 immunofluorescence (right) 48 hours after *Pou5f1 cDNA* transfection migrated much farther from the explant than control cells transfected with *pcDNA* empty vector or pcDNAGFP vector, thus revealing their EndMT competency and invasive potential. In contrast, *Pou5f1* antisense inhibited EndMT as scored by the number of cells migrating out the explant. Then, *RelA/p65* (activated NFκB) transfection of endocardial cells increased both number of cells undergoing EndMT and their invasive properties in agreement with previously published data (*18*). Ikkβ that blocks NFκB decreased EndMT. *Pou5f1* antisense also inhibited RelA/p65-induced EndMT (Fig. 7A). Furthermore, *Pou5f1* cDNA–expressing OFT (or AVC) explants cultured for 2 weeks in a chondrogenic medium (*27*) expressed OCN in valvular mesenchymal cells migrating from the explants in contrast to empty *pcDNA* vector–transfected explants (Fig. 7B).

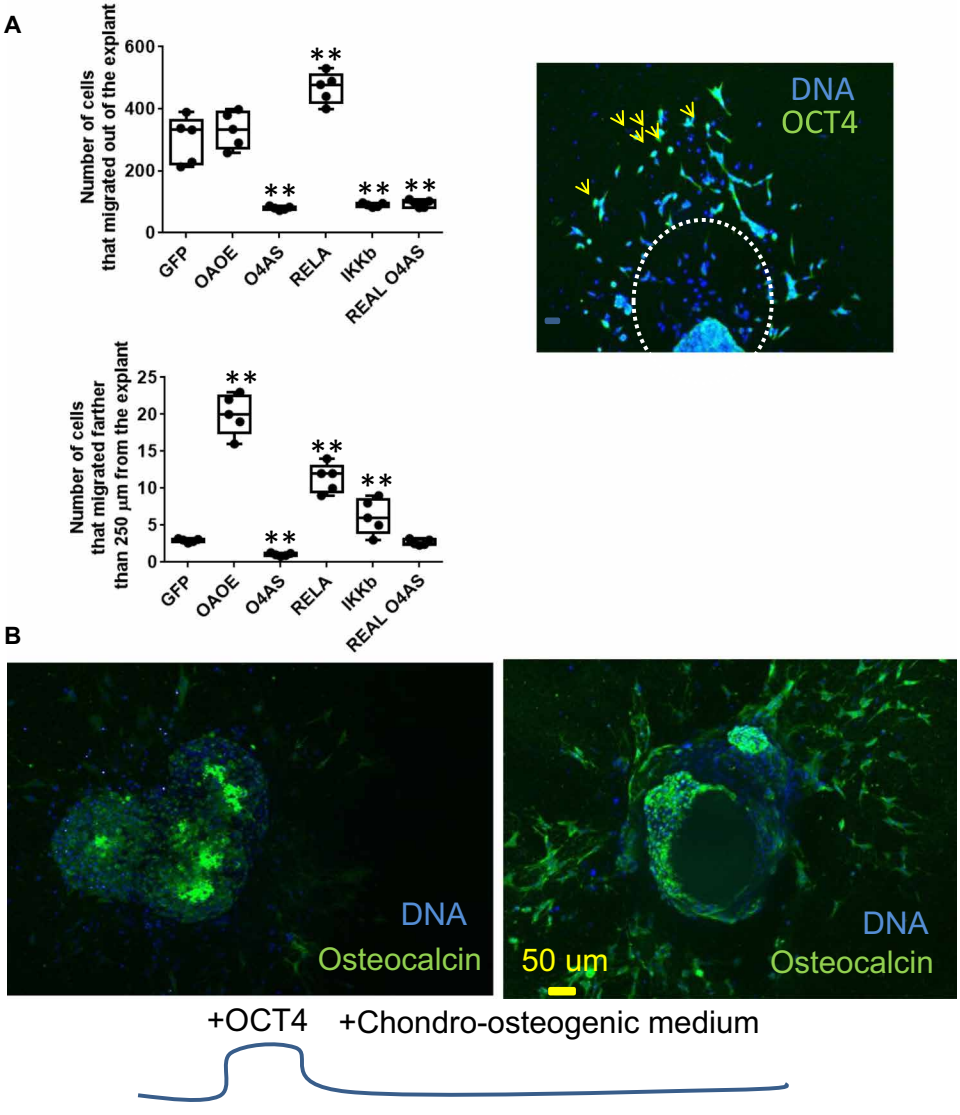

Fig. 7. Oct4 mediates NFκB-induced EndMT and calcification of VEC and VICs. Atrioventricular explants on collagen gels undergoing EMT. *Pou5f1* sense (gain of function O4OE) or antisense (loss of function, O4AS), as well as *RelA* or *IKK*β or *pcDNAGFP (GFP)* or both *RelA* and *Pou5f1* antisense (RelAO4AS) cDNA was injected in the AVC 3 hours before dissection and culture on collagen gels. (**A**) Cells migrating from the explants were scored (top), as well as their distance of migration from the explants (bottom). Right: Image of $OCT4^{+}$ cells (arrows) migrating from the explant. (**B**) Explants were cultured for 18 days with the chondro-osteogenic medium. They were then fixed and immunostained with an anti-OCN antibody. Data are representative of five experiments and are presented as whisker plots (minimum to maximum with the 2.5/97.5 percentile). Comparisons versus GFP were analyzed by Student's *t* test. $^{**}P \leq 0.001$.

Oct4 mediates aortic valve calcification and stenosis in $LDR^{-/-}$ and $ApoE^{-/-}$ mice fed with high-fat diet

We next used a previously established mouse model of aortic valve calcification, the low density lipoprotein (LDL)–receptor knockout mice fed for 4 months with a high-fat diet (*15*). Similar to the human aortic valve, virtually no expression of Oct4 was found in the valves of adult wild-type mice, and none are nuclear active (Fig. 8, A and B).

We next tested whether deactivation of NFκB could result in less Oct4 expression and/or activity in leaflets in vivo. We generated $LDR^{-/-}$ mice with valve-specific down-regulation of NFκB via $NFATc1^{enCre}$: $IKKb^{fl/fl}$ (*15*) fed with high-fat diet for 4 months. We determined that unlike $LDLr^{-/-}$ valves (Fig. 8B), down-regulation of NFκB activity in conditionally deleted valves via $IKKb^{-/-}$ resulted in substantial down-regulation of OCT4 (Fig. 8B), although not quite to wild-type levels.

As OCT4 was found in both human and mouse calcified valve and triggered calcification of both adult VICs and embryonic valvular cells, we then tested whether deletion of *Pou5f1* in the endocardium could prevent calcification in adult $Apoe^{-/-}$ mice fed with high-fat diet, another mouse model of aortic valve calcification. $Tie2^{cre+/-}$ / $Pou5f1^{flox/flox}/Apoe^{-/-}$ mice were fed for 6 months with a high-fat diet. Aortic velocity monitored by Doppler echocardiography showed that $Pou5f1^{flox/flox}/Apoe^{-/-}$ mice featured extreme ejection velocities (up to 3 m/s) also accompanied with regurgitation (Fig. 8C), consistent with extreme hemodynamic aortic stenosis (*28*). Aortic velocity, however, was normal according to standard values (~1 m/s) (*29*) in

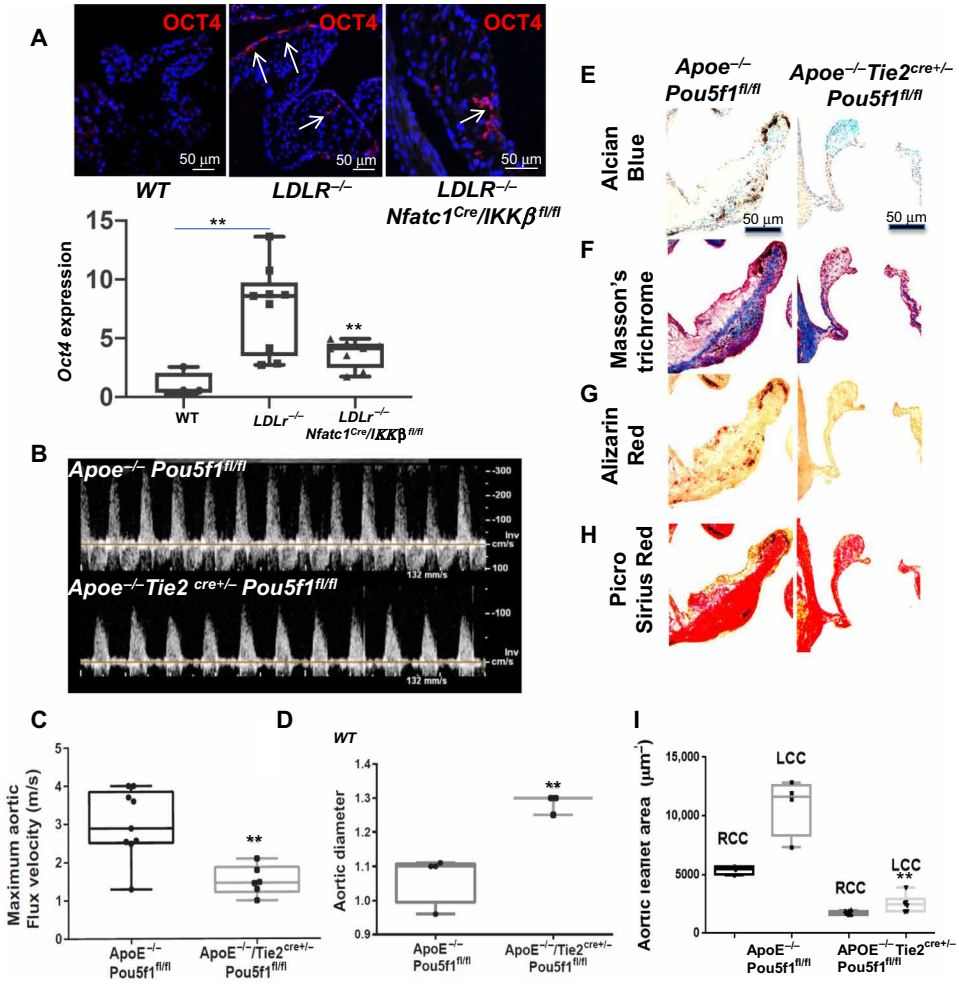

Fig. 8. Oct4 mediates aortic valve calcification and stenosis in adult mice. (**A**) *Ldlr*$^{-/-}$ + high-fat diet induced elevated OCT4 expression in murine aortic valve. Valve-specific down-regulation of NFκB via *NFATc1*^{enCre}*:IKKβ*$^{fl/fl}$ resulted in down-regulation of Oct4 in the *Ldlr*$^{-/-}$ + high-fat diet background. Top: Anti-Oct4 immunofluorescence in aortic valve of *wt*, *ldlr*$^{-/-}$ and *ldlr*$^{-/-}$*/Nfatc1*^{enCre}*:IKKb*$^{fl/fl}$ mice. Bottom: Graph showing expression of Oct4 in the three mouse models. (**B** to **D**) Doppler echocardiography recording of high-fat fed *Apoe*$^{-/-}$ *Pou5f1*$^{flox/flox}$ male mice and of male *Apoe*$^{-/-}$*/Tie2*$^{cre+/-}$*Pou5f1*$^{flox/flox}$ mice with a deletion of *Pou5f1* in the endocardial lineage. (B) Representative recordings of the aortic flux revealing high aortic flux and aortic valve regurgitation in the *Apoe*$^{-/-}$ genetic background in the presence but not in the absence of *Oct4* deleted via *Tie2*$^{cre+/-}$*/Pou5f1*$^{flox/flox}$. (C) Graph showing aortic velocity ($n = 6$). (D) Graph showing aortic diameter. (E to **I**) Murine aortic valves with postgastrulation down-regulation of Oct4 in endothelial lineages via *Tie2*$^{cre+/-}$*/Pou5f1*$^{flox/flox}$ show reduced thickening, retention of collagen/glycosaminoglycan striation, and no calcified lesion formation compared with *Pou5f1*$^{flox/flox}$ mice aortic valves in the *Apoe*$^{-/-}$ background. Alcian Blue (E), Masson's trichome (F), Alizarin Red (G), and Picro Sirius Red (H). Images are representative of six mice. (I) Aortic leaflet areas, right and left coronary cusp (RCC and LCC). Data are presented as whisker plots (minimum to maximum with the 2.5/97.5 percentile). Comparisons were analyzed by Student's *t* test and ANOVA ($n = 6$). **$P \leq 0.001$.

Tie2$^{cre+/-}$/*Pou5f1*$^{flox/flox}$/*Apoe*$^{-/-}$ mice (Fig. 8D). The aortic diameter monitored in the proximal region was also significantly decreased in *Pou5f1*$^{flox/flox}$/*Apoe*$^{-/-}$ mice when compared with *Tie2*$^{cre+/-}$/*Pou5f1*$^{flox/flox}$/*Apoe*$^{-/-}$ (Fig. 8E), further establishing that deletion of Oct4 in the endothelial lineage prevented aortic stenosis. The histology of aortic valves using Masson trichrome staining, Alcian Blue to specifically stain glycosaminoglycans usually enriched in cartilage cells, Sirius red to stain collagen, and Alizarin Red that marks $Ca2^{+}$ deposition in both groups of mice first confirmed that *Apoe*$^{-/-}$ aortic valve featured both fibrosis and calcification (Fig. 8, E to I). This was accompanied with an enlargement of both the right and the left coronary cusps (Fig. 8I). In contrast, aortic valve of *Tie2*$^{cre+/-}$/*Pou5f1*$^{flox/flox}$/*Apoe*$^{-/-}$ showed much less glycosaminoglycans and collagen, no Ca^{2+} deposition, and no thickening (Fig. 8, E to I). Together, these data reveal that Oct4 mediates NFκB-induced EndMT and drives valvular cells toward an osteogenic cell fate, which can be prevented by local inhibition of *Oct4*.

We further tracked the *Oct4* cell lineage in calcified aortic valves. *Pou*^{creERT2}/*Rosa26*^{tdT}/*Apo*E$^{-/-}$ mice were born from a mother in which the recombinase cre had been induced at E8.0 during gestation. At 6 weeks old, these mice were fed for 4 months with high-fat diet. Figure S6 shows that tomato^{+} cells feature a deposition of OCN protein.

DISCUSSION

Together, our genetic lineage tracing findings identify that postgastrulation Oct4^{+} cells originate from the anterior pharyngeal endoderm, a region in close contact to E8.0 embryos (*30*), possibly

contributing to the endocardium, as well as adjacent to the OFT at later stage. The cells migrate into the OFT (*31*, *32*) to contribute to formation of the valve endocardium both in OFT and AVC. The single-cell RNA-seq analysis of *Pou5f1*^{CreERT2}/*Rosa26*^{tdTomato}-sorted cells revealed a rare but important subset of Oct4$^+$-derived endocardial cells that acquire EndMT competency and are at the origin of chondro-osteogenic progenitors in semilunar and atrioventricular valves. Several pieces of data point that at least part of Oct4$^+$-derived cells likely originate from the pharyngeal endoderm close to the OFT, a region reported to contribute to the formation of the OFT and the aortic valve (*33*). First, tomato$^+$ cells from *Pou5f1*^{creERT2}/*Rosa26* ^{tdT} were found in this region (Fig. 5) and look to migrate through the OFT into the chambers. Second, single-cell RNA-seq from the same cells both at E9.5 and E10.5 revealed clusters of cells expressing gene markers of the pharyngeal endoderm. These cells further express genes that confer them migratory and invasive properties (Fig. 6 and fig. S6). The presence of tomato$^+$ cells in postnatal valves originating from OCT4$^+$ earlier progenitor cells further suggests that these cells could be reactivated and be at the origin of calcifying cells in adults. This was confirmed by the presence of tomato cells in adult calcifying aortic valve expressing OCN (fig. S7).

The different stages of EndMT with cells expressing both endothelial and mesenchymal genes (early to late hybrid cells) that were captured in our single-cell analysis likely reflect the slight variability in the age of the embryos selected from 18 to 20 somites from six different E9.5 embryonic litters, a stage of development at which EndMT of endocardial cells has started to form the valve cushions. Our data thus reflect the dynamic process of EndMT within the time frame between 18 and 20 somites that is pursued heterogeneously by both the pharyngeal endodermal cell and the endocardial cells populations.

Overall, our comprehensive set of data identified a novel population of early OCT4$^+$ valvular progenitors in endodermal/endocardial cells competent for EndMT. These cells are further pushed forward to undergo EndMT by NFkb as demonstrated by studies using explants deficient in NFkb signaling pathway (Fig. 7). The cells then contribute to cardiac cushions and, in turn, to a subset of osteochondral VICs (*27*, *34*).

We found a functional OCT4 in nuclei of human calcified aortic valvular cells. We used *LDLR*$^{-/-}$ and *Apoe*$^{-/-}$ genetically modified mice, both models of valve calcification, although they may feature some limitations such as not progressing toward a fully calcified valve. VEC and, in turn, VIC deficient in *NFκB* or in *Oct4* in loss-of-function experiments revealed that OCT4 induced by NFκB is required in the process of aortic valve disease (Fig. 8).

Our single-cell data targeting a rare cell population within the pharyngeal endoderm and the endocardium, the AVC, and OFT of E9.5 embryos and lineage-tracing experiments both predicted that the embryonic chondro-osteogenic progenitor cells expressing markers of stem cell pluripotency could be at the origin of calcification in adults. This hypothesis was further documented by the fact that Oct4 when expressed in adult VIC targets mostly regulatory regions of genes involved in EndMT and calcification (Fig. 4). NFκB activation by TNFα or direct expression of RelA in VEC was also found upstream and inductive of OCT4 both in vitro (Fig. 3) and ex vivo (figs. S2 and S3). OCT4 then, in turn, drives EndMT and mesenchymal reprogramming to a progenitor phenotype (Fig. 2). The ancient transcription factor further mediates NFκB-induced cell calcification in cells cultured in the inflammatory OGM (fig. S3). Thus, NFκB-transformed and NFκB-reprogrammed VEC expressing OCT4 and stem cell pluripotency genes will ultimately lead to calcification. Our data (fig. S5) further suggest that the estrogen receptor estrogen related receptor alpha (ERRα) and the Wnt pathway both known to interact via ERRβ or directly (*35*–*37*), respectively, with OCT4 may play both cell reprogramming (our data) and calcifying roles as recently described (*25*).

Together, these findings revealed that OCT4 is a key player within an inflammatory pathway in the process of valve calcification. While OCT4 was found to be expressed in some pathological situations (*38*–*40*), our findings bring a cell origin and a molecular mechanism that explain the role of OCT4 in a pathological process.

We further investigated how both NFκB and its target OCT4 trigger this process. We uncovered that VICs challenged in the course of an NFκB-dependent inflammatory process reexpress OCT4 at the adult stage, possibly following a memory-based epigenetic mechanism. The Pou factor that primes endocardial cells toward EndMT and then chondro-osteogenic cells early in development likely switches back the embryonic osteogenic transcriptional program in the adult somatic cell. This demonstrates that OCT4 is capable of reversing the somatic valvular cells in a more plastic state likely by remodeling the nuclear chromatin (*14*).

In line with this hypothesis, our data uncovered *Runx1* (the only Runx transcription family gene annotated in pig genome) as a target of Oct4 (Fig. 3). Furthermore, Oct4 turns on a stem cell pluripotency gene program including genes such as *Bmi1*, which like *Pou5f1* are sufficient to reprogram somatic cells (*41*, *42*) both in embryonic valvular progenitor and adult valvular cells as revealed by their transcriptomic profiles (Fig. 2 and fig. S4) in line with its reprogramming function.

How NFκB could turn on *Pou5f1* and the OCT4 protein in somatic embryonic or adult valvular cells at a stage when chromatin around *pou5f1* is closed is another open question. It could act as a pioneer factor as suggested (*43*) and activate superenhancers as previously shown (*44*), such as the one of *Pou5f1* (*45*). Alternatively, it could be recruited by another pioneer factor of the GATA family including GATA4, GATA5, and GATA6 (*46*) or of the ETS Variant Transcription factor 6 (ETV) transcription factor family including *Etv2* or *ERG* (*44*), the latter playing a key role in EndMT (*47*). Most of these factors are expressed in embryonic endocardial cells (Fig. 6B) and in adult VECs (*47*, *48*).

Innate immunity, required for nuclear reprogramming (*49*) and mediated by the master transcription factor NFκB, likely plays a key role in the OCT4-dependent VIC reprogramming process leading to osteogenic cells.

In summary, Pou5f1 (Oct4) and, more broadly, the POU family belong to a class of ancient transcription factors. Although highly conserved during evolution (*50*), their function has gained diversity. Our study revealed a novel function of the gene in a yet not well-understood process of valve formation and calcification. OCT4 plays its role in both aortic and potentially mitral valves [i.e., more specifically the mitral annulus originating from both epicardial cells differentiating in AV cushion cells and likely some AVC endocardial cells; (*51*)]. Furthermore, prevention of NFkb-dependent inflammatory pathway or inactivation of OCT4 indicates a pathway toward a therapeutic anticalcification strategy.

METHODS

Human aortic valves

Sclerotic and calcified human valves were obtained from patients undergoing valve replacement surgery at Robert Packer Hospital in

Sayre, PA. Patient age range was 65 to 90 years, with mean age of 76.2 years (21 participants). The Institutional Review Board (IRB) at Seattle Children's Hospital, Guthrie IRB at Robert Packer Hospital, and the IRB for Human Participants at Cornell University approved all procedures (IRB no. 0908-24, gene expression and phenotypic changes in stenotic aortic valves). Written informed consent was obtained from all participants.

Mice

Tie2$^{cre+/-}$, *Pou5f1*^{creERT2,} *Rosa26*^{tdtomato}, *LDLr*$^{-/-}$, *and Apoe*$^{-/-}$ were obtained from the Jackson Laboratory. *Pou5f1*$^{flox/flox}$ mice were obtained from Schöler's laboratory (Munster University, Germany). *Nfatc*^{Cre} (Nfatc1-enhancer Cre, *Nfatc1*^{enCre}) mice were provided by B. Zhou laboratory (Albert Einstein College of medicine, New York); Ikkβ floxed mice were given by M. Karin Laboratory (University of California, San Diego, La Jolla). Mice were kept under standardized conditions (22° to 24°C temperature; 50 ± 20% humidity) on a 12-hour light/12-hour dark cycle in an enriched environment (kraft paper enrichment). Food and tap water were provided ad libitum. *LDLr*$^{-/-}$, *or Apoe*$^{-/-}$ male mice were fed at the age of 2 months with a 45% fat diet for 4 months, including sucrose butter, casein, cornstarch di-calcium phosphate calcium carbonate sodium chloride potassium sulfate, magnesium oxide, and cholesterol. Fat was 17.5% fat protein, 21% raw fat oil, and 3% fat fibers (Safe Diet, France).

Tie2$^{cre+/-}$ *or* Pou5f1^{creERT2} mice (2- to 4-month-old males) were bred with 3-month-old Rosa26^{tdTomato} female mice. Tamoxifen (20 μg/g; mouse) was given to Rosa26^{tdTomato} female mice bred with Pou5f1^{creERT2} (2 to 4 months old) males by oral gavage.

DNA injection in embryos and OFT and AVC explants

DNA [plasmids encoding *Pou5f1*, *Pou5f1* antisense (*13*), *IKK*β, *RelA:p65* (*15*), *or* empty *pcDNA* vector, or *pcDNA GFP* vectors used as controls] was mixed with lipofectamine according to the manufacturer's protocol. The injection pipette was filled with the transfection mix and injected into the lumen of the OFT or AVC of the embryos. The embryos were cultured for 3 hours in the presence of BDM (1 mM) to prevent heart contraction as previously described (*52*).

AVCs and proximal OFTs were then dissected from E9.5 and E10.5 mouse embryos, respectively, and transferred to a collagen gel as previously described (*52*). EndMT was scored in the next 48 hours as both the number of cells that migrated out of the explant and the distance of migration using Image J.

Valvular endothelial and interstitial cell culture and transfection

Porcine aortic valve cusps were cut and washed in sterile phosphate-buffered saline for at least five times before cell isolation. Aortic valves were incubated for 10 min in collagenase (2 mg/ml; CLS type II Gibco) solution prepared in fresh cell culture medium [Dulbecco's modified Eagle's medium (DMEM)] (Thermo Fisher Scientific, France) and 10% fetal bovine serum [FBS; Atlanta Biologicals (USA) or Eurobio, (France)] added with penicillin/streptomycin, at 37°C under a humidified atmosphere and 5% CO_2. VECs were removed by scraping the surface of the cusps after 15 min of incubation and collected by centrifugation at 800 revolutions per minute for 4 min. Harvested pig aortic valvular endothelial cells (PAVECs) were cultured in heparin medium [heparin (50 U/ml), Sigma-Aldrich] in DMEM, 10% FBS, and penicillin/streptomycin at 37°C under a humidified atmosphere and 5% CO_2. After VEC removal, aortic valves were further incubated with collagenase overnight for VIC isolation. VICs were then cultured in complete cell culture medium (DMEM, 10% FBS, and penicillin/streptomycin) at 37°C under a humidified atmosphere and 5% CO_2.

Gene expression was monitored in reverse transcription quantitative PCR (RT-Q-PCR) as previously described (*45*). PCR primers are listed in Table 1.

3D hydrogel culture model preparation

3D collagen hydrogels with porcine aortic valve interstitial and endothelial cells were created as described previously (*21*). Briefly, VICs were trypsinized and resuspended at a concentration of 1 million cells/ml in a collagen solution (2 mg/ml) supplemented with 10% FBS and neutralized with NaOH. Two hundred microliters of this VIC gel solution was pipetted into individual wells of a 24-well plate. Each well of the plate was previously lined with a barrier of hydrophobic pen (ImmEdge, Vector Labs) to create a gel bolus in the center of the well. The VIC gel and cell-free gel were allowed to polymerize in the incubator at 37°C for more than 30 min. For VEC culture, VECs were seeded on the surface of the cell-free gel at a density of 100,000 cells/cm^2. For osteogenic growth media (OGM), basal medium was supplemented with 10 mM β-glycerophosphate, L-ascorbic acid (50 μg/ml), and 100 nM dexamethasone. Gels were cultured for 14 days with media changed every 48 hours.

Plasmid transfection

Plasmids were delivered to VEC or VIC using the 100-μl Neon Transfection System (Life Technologies) according to the manufacturer's

Table 1. Real-time PCR primers used for porcine genes.

Primer	Forward sequence (5′ to 3′)	Reverse sequence (5′ to 3′)
18s	AATGGGGTTCAACGGGTT	TAGAGGGACAAGTGGCGT
ACTA2	CAGCCAGGATGTGTGAAGAA	TCACCCCCTGATGTCTAGGA
RUNX2	GCACTACCCAGCCACCTTTA	TATGGAGTGCTGCTGGTCTG
OCN	CTCCAGCCACAACATCCTTT	TGGCCTCCAGCACTGTTTAT
POU5F1	GCAGTGACTATTCGCAACGA	TAGCCTGGGGTACCAAAATG
SNAIL1	GCCCAACTACAGCGAGCTAC	CCAGGAGAGAGTCCCAGATG
VE-CAD	CGTGGTGGAAACACAAGATG	TGTGTACCTGGTCTGGGTGA

instructions and as previously described (*53*). Electroporation conditions were 1600 V, 20 ms, and 1 pulse. Plasmids expressing Oct4 and an antisense sequence for inhibition of Oct4 activity were previously published (*13*). Plasmids expressing *RelA/p65* and *IkkB* were previously described (*15*).

Ex vivo aortic valve leaflet organ culture

Porcine hearts were obtained from Shirk Meats (Dundee, NY), and the aortic valve leaflets were extracted sterilely. Following extraction, the leaflets were rinsed in sterile PBS and cultured in DMEM. DMEM was supplemented with 10% FBS and 1% penicillin-streptomycin or supplemented with OGM as previously described. The medium was changed every 48 hours for 21 days (*17*).

Histology and immunofluorescence analysis

Adult mouse hearts or hydrogel cultures were fixed in 4% paraformaldehyde overnight at 4°C, then dehydrated with a series of ethanol washes, and embedded in paraffin. The blocks were sectioned at a thickness of 8 μM. Sections were stained with Alcian Blue (glycosaminoglycans), Masson's trichrome (collagen fibers), Alizarin Red (calcium), and Picrosirius Red (collagen) according to the manufacturer's instructions. Images were obtained with the Olympus upright BX-50 microscope (Center Valley, PA). Staining intensity was measured using ImageJ (NIH, Bethesda, MD) using the ImageJ plugin Colour Deconvolution to separate channels, and all values were normalized to total valve area. Alternatively, bound Alizarin Red dye was released from the gels and measured via colorimetry. Immunofluorescence staining of cells in whole mount or in thin sections was completed as described previously (*54*). Images were obtained with the Zeiss 710 (Thornwood, NY) laser scanning confocal microscope.

In some experiments, E10.5 Pou5f1^{creERT2} × Rosa26^{tdTomato} embryos were fixed overnight in 10% formaldehyde, washed with PBS, permeabilized in PBS 2% Tween 20 for 3 hours, and transparized using Rapiclear 1.52 (Sunjin laboratory) for 15 min. Embryos were imaged using a 10× long-distance [numerical aperture (NA), 0.45] objective.

Doppler ultrasound transthoracic echocardiography

Echocardiography was performed using an Affiniti 50 (Philips) and a 15-MHz probe. Mice were anesthetized with 4% isoflurane and maintained under 1 to 1.5% isoflurane. Aortic flow was monitored using PW Doppler-mode by positioning the Doppler sample volume parallel to flow direction, assisted by Color Doppler-mode. Echocardiographies were analyzed blinded by a cardiologist who had not performed the recordings. A minimum of six mice in groups were monitored.

ChIP assay

ChIP assay was performed from chromatin extracted from VIC nucleoporated with *Pou5f1* cDNA cloned in a pcDNA vector using Amaxa electroporator (Amaxa, France). Green fluorescent protein (GFP)–transfected cells were imaged 24 hours later to check transfection efficiency just before the preparation of chromatin (Fig. 2B, inset). Chromatin was prepared, and anti-Oct4 immunoprecipitation was performed as previously described (*55*). Both unprecipitated (input) and precipitated DNA were used in real-time PCR (Roche LC1.5) using SYBR green reagent (Roche) or amplified within a library and sequenced using a NextSeq Illumina sequencer. Enrichment of Oct4 on genomic sites was calculated as percentage of input. Primers are listed in Table 2.

Fastq files were aligned to the pig (susScr11) reference genome, PCR duplicates were removed using Samtools, and normalized genome coverage tracks were generated from uniquely mapping reads (mapq >30) using deepTools2. Single-end reads, unmated reads, and mate reads that map too far apart (>4× fragment length) were extended by 200 base pairs (bp). Biological replicates were pooled, and coverage was then calculated as average reads per million of mapped reads in 10-bp bins. To determine the peaks for ChIPs with narrow binding profiles, datasets were uniformly processed using the MACS2 with default parameters.

Single-cell PCR

Tie2^{cre} mice were bred with Rosa26^{tdTomato} mice. AVC and OFT were dissected out and enzymatically dissociated using TrypLE (Thermo Fisher Scientific, France). Tomato^{+} cells were collected under an epifluorescence microscope using a micropipette. Each collected cell was transferred to a PCR tube containing 5 μl of cell lysis buffer (Roche). Reverse transcription (RT) was performed in 10-μl reaction volume using an AffinityScript Multiple Temperature cDNA synthesis kit (Agilent, France). A 10-cycle pre-PCR was carried out in 20 μl of reaction mixed (polymerase NEB). The mix was diluted three times, and 2 μl was run in real-time PCR (Roche LC1.5) using SYBR green reagent (Roche). PCR of β-*actin* used as a housekeeping gene was first run to normalize the RNA amount before running the *Pou5f1* PCR. Primers are listed in Table 3.

Single-cell RNA-seq

Pou5f1^{creERT2} mice were bred with Rosa26^{tdTomato} mice. Tamoxifen (20 μg/g; mouse) was injected at E7.5 and E8.0. Embryos were collected

Table 2. ChIP-PCR primers used for pig and human gene regulatory regions.

Primer	Forward sequence (5′ to 3′)	Reverse sequence (5′ to 3′)
PIG RUNX1	AGCAATTCAACGTTGGCACC	CACCAAGAACCCAGCTCTCC
PIG HAPLN1	ATGGTTATGCCCACAATCCCA	TGGGGGAGAAAAGCCATTTGA
PIG RUNXTL1	GCCCCAGGACCCTTCTCTAA	AGCCTCACAGTATCACTGCCAC
PIG RUNX2	GGGGAAACTTGACCATGGGA	CCAACCTGGCCCAAGAAAAC
PIG MSX2	GGGCTGCGCTTGAATTATGA	TTTGTTATTCGGAGGCGGGA
PIG SP7	ACACCGGATCCTCAACTGAC	ATTCTGGAGCCCCTTGTTTT
HUMAN *OCT4* enhancer	AGCTGCTCCCTTATGCCTTC	TATAGCACGGAGGCCTTGTC

Table 3. Real-time PCR primers used for mouse genes in single-cell PCR.

Primer	Forward sequence (5′ to 3′)	Reverse sequence (5′ to 3′)
Pou5f1	CGCCGGTTACAGAACCAT	AAGTGGGTGGAGGAAGCC
β-*Actin*	TGACCCTGAAGTACCCCATTGA	CTGGGTCATCTTTTCACGGTT

at E9.5 or E10.5. AVCs, OFT, and adjacent heart forming field region were dissected out from 60 E9.5 and 48 E10.5 mouse embryos and enzymatically dissociated using TrypLE (Thermo Fisher Scientific, France) in the presence of 100 nM thiazovivin. Cells were filtered through a 40-μm mesh and FACS sorted, and cells were processed in Chromium (10X genomics). cDNA libraries were sequenced with a NextSeq Illumina sequencer. A first analysis was performed with cell Ranger and C-loop 10X genomics softwares. Then, a secondary analysis was done using the computational workflow SCHNAPPS (*56*), developed by B. Jagla at Pasteur Institute, Paris. Data were normalized using a global-scaling normalization method "LogNormalize." To cluster the cells, we used the SCRAN algorithm and the igraph method. We use principal components analysis for performing a predimensionality reduction before running the t-SNE plotting. We thus choose 50 components, a number of variable genes of 500, and a minimal size of clusters of 50 cells. Trajectory inference was performed using Elpigraph included within the SCHNAPPS computer program (*57*).

Antibodies

Antibodies used for cell or embryo immunofluorescence were raised against Oct4 biotin-conjugated [Santa Cruz Biotechnology, sc-5279 used at 1/200 detected by FITC-conjugated avidin (Santa Cruz Biotechnology)], or Cell Signaling Technology #2750 detected with Alexa-conjugated secondary antibodies, against sarcomeric actinin monoclonal (Sigma-Aldrich France ascites fluid EA-53, used at 1/2000), Runx2 (Abcam, ab7695), NFκB (Cell Signaling Technology, 8242; 1/200; and Santa Cruz Biotechnology, sc-8008 for ChIP; 1 μg/100 μg chromatin), αSMA (Abcam, ab7817, 1/100), and OCN (Abcam, ab13418, 1/100) and anti-CD31 (Pecam, anti-mouse Pharmingen #550274; 1/200; or anti-human Cell Signaling Technology, 3528; 1/400).

Cell imaging

Images were acquired using a confocal LSM 800 Zeiss microscope equipped with an airyscan of 32 detectors. Light was provided by a laser module 405/488,561 and 640-nm wavelengths, respectively.

To visualize cells of embryonic explants, tiles and stacks of images were acquired using a Zeiss observer epifluorescence microscope using a Plan-Apochromat 20× objective. Light was provided by a Colibri 7 source. Number and distance of migrating cells were scored using ImageJ.

All images were acquired using the ZEN ZEISS software. Then, some images were deconvoluted using Autoquant and reconstructed in 3D using Imaris software (IMARIS). All samples were mounted in Fluoromount (Cliniscience, France).

Statistical analysis

Data are expressed as means ± SEM or as minimum to maximum and 2.5 to 97.5 percentile as mentioned in each figure. In all experiments, data were compared between two groups with Student's *t* tests, and those with three and more groups with analysis of variance (ANOVA) and Tukey's post hoc pairwise testing using GraphPad Prism. A P value ≤ 0.05 was considered to be statistically significant. A minimum of three and six biological replicates were performed for in vitro experiments and for ex vivo and in vivo experiments, respectively. In vivo experiments were mostly blinded. Echocardiographic recordings were analyzed by two independent researchers and clinicians. Histology in Fig. 8 was performed by blinded researchers at Cornell University from samples sent by the INSERM laboratory after mice echocardiography monitoring.

Animal experiments

The animal experiments in France were performed according to the guidelines from Directive 2010/63/EU of the European Parliament on the protection of animals used for scientific purposes. Animal experiments were approved by the French Ministry of Agriculture (project #20843) and the local Ethics committee of Aix-Marseille University. In the United States, the mouse experiments were performed under the Institutional Animal Care and Use Committee protocol #2008-0011.

SUPPLEMENTARY MATERIALS

Supplementary material for this article is available at https://science.org/doi/10.1126/sciadv.abf7910

View/request a protocol for this paper from *Bio-protocol*.

REFERENCES AND NOTES

1. L. Chappell, A. J. C. Russell, T. Voet, Single-cell (multi)omics technologies. *Annu. Rev. Genomics Hum. Genet.* **19**, 15–41 (2018).
2. M. D. Combs, K. E. Yutzey, Heart valve development: Regulatory networks in development and disease. *Circ. Res.* **105**, 408–421 (2009).
3. R. B. Hinton, K. E. Yutzey, Heart valve structure and function in development and disease. *Annu. Rev. Physiol.* **73**, 29–46 (2011).
4. S. Chakraborty, M. D. Combs, K. E. Yutzey, Transcriptional regulation of heart valve progenitor cells. *Pediatr. Cardiol.* **31**, 414–421 (2010).
5. J. I. Hoffman, Congenital heart disease: Incidence and inheritance. *Pediatr. Clin. North Am.* **37**, 25–43 (1990).
6. V. T. Nkomo, J. M. Gardin, T. N. Skelton, J. S. Gottdiener, C. G. Scott, M. Enriquez-Sarano, Burden of valvular heart diseases: A population-based study. *Lancet* **368**, 1005–1011 (2006).
7. N. M. Rajamannan, Calcific aortic valve disease: Cellular origins of valve calcification. *Arterioscler. Thromb. Vasc. Biol.* **31**, 2777–2778 (2011).
8. J. D. Hutcheson, M. C. Blaser, E. Aikawa, Giving calcification its due: Recognition of a diverse disease: A first attempt to standardize the field. *Circ. Res.* **120**, 270–273 (2017).
9. N. M. Rajamannan, F. J. Evans, E. Aikawa, K. J. Grande-Allen, L. L. Demer, D. D. Heistad, C. A. Simmons, K. S. Masters, P. Mathieu, K. D. O'Brien, F. J. Schoen, D. A. Towler, A. P. Yoganathan, C. M. Otto, Calcific aortic valve disease: Not simply a degenerative process: A review and agenda for research from the National Heart and Lung and Blood Institute Aortic Stenosis Working Group. Executive summary: Calcific aortic valve disease-2011 update. *Circulation* **124**, 1783–1791 (2011).
10. G. A. Walker, K. S. Masters, D. N. Shah, K. S. Anseth, L. A. Leinwand, Valvular myofibroblast activation by transforming growth factor-beta: Implications for pathological extracellular matrix remodeling in heart valve disease. *Circ. Res.* **95**, 253–260 (2004).
11. A. C. Liu, V. R. Joag, A. I. Gotlieb, The emerging role of valve interstitial cell phenotypes in regulating heart valve pathobiology. *Am. J. Pathol.* **171**, 1407–1418 (2007).

12. J. Nichols, B. Zevnik, K. Anastassiadis, H. Niwa, D. Klewe-Nebenius, I. Chambers, H. Schöler, A. Smith, Formation of pluripotent stem cells in the mammalian embryo depends on the POU transcription factor Oct4. *Cell* **95**, 379–391 (1998).
13. D. Zeineddine, E. Papadimou, K. Chebli, M. Gineste, J. Liu, C. Grey, S. Thurig, A. Behfar, V. A. Wallace, I. S. Skerjanc, M. Pucéat, Oct-3/4 dose dependently regulates specification of embryonic stem cells toward a cardiac lineage and early heart development. *Dev. Cell* **11**, 535–546 (2006).
14. N. Abboud, T. M. Morris, E. Hiriart, H. Yang, H. Bezerra, M.-G. Gualazzi, S. Stefanovic, A.-C. Guénantin, S. M. Evans, M. Pucéat, A cohesin-OCT4 complex mediates sox enhancers to prime an early embryonic lineage. *Nat. Commun.* **6**, 6749 (2015).
15. T. Gee, E. Farrar, Y. Wang, B. Wu, K. Hsu, B. Zhou, J. Butcher, NFκB (nuclear factor κ-light-chain enhancer of activated B cells) activity regulates cell-type-specific and context-specific susceptibility to calcification in the aortic valve. *Arterioscler. Thromb. Vasc. Biol.* **40**, 638–655 (2020).
16. C. J. Holliday, R. F. Ankeny, H. Jo, R. M. Nerem, Discovery of shear- and side-specific mRNAs and miRNAs in human aortic valvular endothelial cells. *Am. J. Physiol. Heart Circ. Physiol.* **301**, H856–H867 (2011).
17. E. J. Farrar, G. D. Huntley, J. Butcher, Endothelial-derived oxidative stress drives myofibroblastic activation and calcification of the aortic valve. *PLOS ONE* **10**, e0123257 (2015).
18. D. M. DeLaughter, D. C. Christodoulou, J. Y. Robinson, C. E. Seidman, H. S. Baldwin, J. G. Seidman, J. V. Barnett, Spatial transcriptional profile of the chick and mouse endocardial cushions identify novel regulators of endocardial EMT in vitro. *J. Mol. Cell. Cardiol.* **59**, 196–204 (2013).
19. G. J. Mahler, E. J. Farrar, J. T. Butcher, Inflammatory cytokines promote mesenchymal transformation in embryonic and adult valve endothelial cells. *Arterioscler. Thromb. Vasc. Biol.* **33**, 121–130 (2013).
20. E. J. Farrar, J. T. Butcher, Heterogeneous susceptibility of valve endothelial cells to mesenchymal transformation in response to TNFα. *Ann. Biomed. Eng.* **42**, 149–161 (2014).
21. J. Richards, I. el-Hamamsy, S. Chen, Z. Sarang, P. Sarathchandra, M. H. Yacoub, A. H. Chester, J. T. Butcher, Side-specific endothelial-dependent regulation of aortic valve calcification: Interplay of hemodynamics and nitric oxide signaling. *Am. J. Pathol.* **182**, 1922–1931 (2013).
22. A. Graham, M. Okabe, R. Quinlan, The role of the endoderm in the development and evolution of the pharyngeal arches. *J. Anat.* **207**, 479–487 (2005).
23. J. J. Quinn, M. G. Jones, R. A. Okimoto, S. Nanjo, M. M. Chan, N. Yosef, T. G. Bivona, J. S. Weissman, Single-cell lineages reveal the rates, routes, and drivers of metastasis in cancer xenografts. *Science* **371**, eabc1944 (2021).
24. I. Pastushenko, A. Brisebarre, A. Sifrim, M. Fioramonti, T. Revenco, S. Boumahdi, A. van Keymeulen, D. Brown, V. Moers, S. Lemaire, S. de Clercq, E. Minguijón, C. Balsat, Y. Sokolow, C. Dubois, F. de Cock, S. Scozzaro, F. Sopena, A. Lanas, N. D'Haene, I. Salmon, J.-C. Marine, T. Voet, P. A. Sotiropoulou, C. Blanpain, Identification of the tumour transition states occurring during EMT. *Nature* **556**, 463–468 (2018).
25. C. V. Theodoris, P. Zhou, L. Liu, Y. Zhang, T. Nishino, Y. Huang, A. Kostina, S. S. Ranade, C. A. Gifford, V. Uspenskiy, A. Malashicheva, S. Ding, D. Srivastava, Network-based screen in iPSC-derived cells reveals therapeutic candidate for heart valve disease. *Science* **371**, eabd0724 (2021).
26. L. Ho, R. Jothi, J. L. Ronan, K. Cui, K. Zhao, G. R. Crabtree, An embryonic stem cell chromatin remodeling complex, esBAF, is an essential component of the core pluripotency transcriptional network. *Proc. Natl. Acad. Sci. U.S.A.* **106**, 5187–5191 (2009).
27. K. Balachandran, P. W. Alford, J. Wylie-Sears, J. A. Goss, A. Grosberg, J. Bischoff, E. Aikawa, R. A. Levine, K. K. Parker, Cyclic strain induces dual-mode endothelial-mesenchymal transformation of the cardiac valve. *Proc. Natl. Acad. Sci. U.S.A.* **108**, 19943–19948 (2011).
28. K. Tanaka, M. Sata, D. Fukuda, Y. Suematsu, N. Motomura, S. Takamoto, Y. Hirata, R. Nagai, Age-associated aortic stenosis in apolipoprotein E-deficient mice. *J. Am. Coll. Cardiol.* **46**, 134–141 (2005).
29. M. Vinhas, A. C. Araújo, S. Ribeiro, L. B. Rosário, J. A. Belo, Transthoracic echocardiography reference values in juvenile and adult 129/Sv mice. *Cardiovasc. Ultrasound* **11**, 12 (2013).
30. J. L. McBride, J. C. Ruiz, Ephrin-A1 is expressed at sites of vascular development in the mouse. *Mech. Dev.* **77**, 201–204 (1998).
31. M. V. de la Cruz, C. Sanchez Gomez, M. M. Arteaga, C. Arguello, Experimental study of the development of the truncus and the conus in the chick embryo. *J. Anat.* **123**, 661–686 (1977).
32. R. H. Anderson, S. Mori, D. E. Spicer, N. A. Brown, T. J. Mohun, Development and morphology of the ventricular outflow tracts. *World J. Pediatr. Congenit. Heart Surg.* **7**, 561–577 (2016).
33. H. M. Phillips, C. A. Stothard, W. M. S. Qureshi, A. I. Kousa, J. A. Briones-Leon, R. R. Khasawneh, C. O'Loughlin, R. Sanders, S. Mazzotta, R. Dodds, K. Seidel, T. Bates, M. Nakatomi, S. J. Cockell, J. E. Schneider, T. J. Mohun, R. Maehr, R. Kist, H. Peters, S. D. Bamforth, *Pax9* is required for cardiovascular development and interacts with *Tbx1* in the pharyngeal endoderm to control 4th pharyngeal arch artery morphogenesis. *Development* **146**, dev177618 (2019).
34. J. Hjortnaes, S. E. P. New, E. Aikawa, Visualizing novel concepts of cardiovascular calcification. *Trends Cardiovasc. Med.* **23**, 71–79 (2013).
35. D. L. C. van den Berg, W. Zhang, A. Yates, E. Engelen, K. Takacs, K. Bezstarosti, J. Demmers, I. Chambers, R. A. Poot, Estrogen-related receptor beta interacts with Oct4 to positively regulate Nanog gene expression. *Mol. Cell. Biol.* **28**, 5986–5995 (2008).
36. L. Sun, T. Liu, S. Zhang, K. Guo, Y. Liu, Oct4 induces EMT through LEF1/β-catenin dependent WNT signaling pathway in hepatocellular carcinoma. *Oncol. Lett.* **13**, 2599–2606 (2017).
37. Y. Li, W. Yu, A. J. Cooney, R. J. Schwartz, Y. Liu, Brief report: Oct4 and canonical Wnt signaling regulate the cardiac lineage factor Mesp1 through a Tcf/Lef-Oct4 composite element. *Stem Cells* **31**, 1213–1217 (2013).
38. I. S. Mohiuddin, S. J. Wei, M. H. Kang, Role of OCT4 in cancer stem-like cells and chemotherapy resistance. *Biochim. Biophys. Acta Mol. Basis Dis.* **1866**, 165432 (2020).
39. D. L. Hess, M. R. Kelly-Goss, O. A. Cherepanova, A. T. Nguyen, R. A. Baylis, S. Tkachenko, B. H. Annex, S. M. Peirce, G. K. Owens, Perivascular cell-specific knockout of the stem cell pluripotency gene Oct4 inhibits angiogenesis. *Nat. Commun.* **10**, 967 (2019).
40. G. F. Alencar, K. M. Owsiany, S. Karnewar, K. Sukhavasi, G. Mocci, A. T. Nguyen, C. M. Williams, S. Shamsuzzaman, M. Mokry, C. A. Henderson, R. Haskins, R. A. Baylis, A. V. Finn, C. A. McNamara, E. R. Zunder, V. Venkata, G. Pasterkamp, J. Björkegren, S. Bekiranov, G. K. Owens, Stem cell pluripotency genes klf4 and oct4 regulate complex SMC phenotypic changes critical in late-stage atherosclerotic lesion pathogenesis. *Circulation* **142**, 2045–2059 (2020).
41. J. B. Kim, V. Sebastiano, G. Wu, M. J. Araúzo-Bravo, P. Sasse, L. Gentile, K. Ko, D. Ruau, M. Ehrich, D. van den Boom, J. Meyer, K. Hübner, C. Bernemann, C. Ortmeier, M. Zenke, B. K. Fleischmann, H. Zaehres, H. R. Schöler, Oct4-induced pluripotency in adult neural stem cells. *Cell* **136**, 411–419 (2009).
42. J.-H. Moon, J. S. Heo, J. S. Kim, E. K. Jun, J. H. Lee, A. Kim, J. Kim, K. Y. Whang, Y.-K. Kang, S. Yeo, H.-J. Lim, D. W. Han, D.-W. Kim, S. Oh, B. S. Yoon, H. R. Schöler, S. You, Reprogramming fibroblasts into induced pluripotent stem cells with Bmi1. *Cell Res.* **21**, 1305–1315 (2011).
43. M. Cieslik, S. Bekiranov, Genome-wide predictors of NF-κB recruitment and transcriptional activity. *BioData Min.* **8**, 37 (2015).
44. H. Michida, H. Imoto, H. Shinohara, N. Yumoto, M. Seki, M. Umeda, T. Hayashi, I. Nikaido, T. Kasukawa, Y. Suzuki, M. Okada-Hatakeyama, The number of transcription factors at an enhancer determines switch-like gene expression. *Cell Rep.* **31**, 107724 (2020).
45. J. M. Dowen, Z. P. Fan, D. Hnisz, G. Ren, B. J. Abraham, L. N. Zhang, A. S. Weintraub, J. Schuijers, T. I. Lee, K. Zhao, R. A. Young, Control of cell identity genes occurs in insulated neighborhoods in mammalian chromosomes. *Cell* **159**, 374–387 (2014).
46. M. Tremblay, O. Sanchez-Ferras, M. Bouchard, GATA transcription factors in development and disease. *Development* **145**, dev164384 (2018).
47. P. Vijayaraj, A. le Bras, N. Mitchell, M. Kondo, S. Juliao, M. Wasserman, D. Beeler, K. Spokes, W. C. Aird, H. S. Baldwin, P. Oettgen, Erg is a crucial regulator of endocardial-mesenchymal transformation during cardiac valve morphogenesis. *Development* **139**, 3973–3985 (2012).
48. S. Y. Oh, J. Y. Kim, C. Park, The ETS factor, ETV2: A master regulator for vascular endothelial cell development. *Mol. Cells* **38**, 1029–1036 (2015).
49. J. Lee, N. Sayed, A. Hunter, K. F. Au, W. H. Wong, E. S. Mocarski, R. R. Pera, E. Yakubov, J. P. Cooke, Activation of innate immunity is required for efficient nuclear reprogramming. *Cell* **151**, 547–558 (2012).
50. D. Onichtchouk, Evolution and functions of Oct4 homologs in non-mammalian vertebrates. *Biochim. Biophys. Acta* **1859**, 770–779 (2016).
51. A. Wessels, M. J. B. van den Hoff, R. F. Adamo, A. L. Phelps, M. M. Lockhart, K. Sauls, L. E. Briggs, R. A. Norris, B. van Wijk, J. M. Perez-Pomares, R. W. Dettman, J. B. E. Burch, Epicardially derived fibroblasts preferentially contribute to the parietal leaflets of the atrioventricular valves in the murine heart. *Dev. Biol.* **366**, 111–124 (2012).
52. E. Hiriart, P. van Vliet, R. J. Dirschinger, S. M. Evans, M. Puceat, Cell labeling and injection in developing embryonic mouse hearts. *J. Vis. Exp.* **86**, e51356 (2014).
53. E. J. Farrar, V. Pramil, J. M. Richards, C. Z. Mosher, J. T. Butcher, Valve interstitial cell tensional homeostasis directs calcification and extracellular matrix remodeling processes via RhoA signaling. *Biomaterials* **105**, 25–37 (2016).
54. P. R. Buskohl, R. A. Gould, J. T. Butcher, Quantification of embryonic atrioventricular valve biomechanics during morphogenesis. *J. Biomech.* **45**, 895–902 (2012).
55. I. Jebeniani, J. Leschik, M. Puceat, Epigenetic regulation of cardiac differentiation of embryonic stem cells and tissues. *J. Vis. Exp.* **112**, e53874 (2016).
56. B. Jagla, V. Rouilly, M. Pucéat, M. Hasan, SCHNAPPs-Single Cell sHiNyAPPlication(s). *BioRxiv* 2020.06.07.127274 [Preprint]. 9 June 2020. https://doi.org/10.1101/2020.06.07.127274.
57. L. Albergante, E. Mirkes, J. Bac, H. Chen, A. Martin, L. Faure, E. Barillot, L. Pinello, A. Gorban, A. Zinovyev, Robust and scalable learning of complex intrinsic dataset geometry via ElPiGraph. *Entropy* **22**, 296 (2020).

Acknowledgments: We are very thankful to R. Markwald (University of South Carolina) for the helpful comments on the manuscript and Haliodx (Marseille, France) and the TAGC INSERM facility [Transcriptomic & Genomic Platform Marseille Luminy | TAGC—Theories and Approaches of Genomic Complexity (univ-amu.fr)] for running the single-cell RNA-seq experiments. **Funding:** We are grateful to the Leducq Foundation for funding part of this research within the MITRAL network of excellence and for awarding us for cell imaging facility [M.P.: "Equipement de Recherche et Plateformes Technologiques" (ERPT)]. E.H. was a fellow of the Ministere de La Recherche et des technologies. We thank the NIH for funding (NIH HL128745 and HL143247 to J.T.B.) and the National Science Foundation for the Graduate Research Fellowship Program. **Author contributions:** E.J.F., E.H., A.M., and D.S.P. designed and performed experiments. B.J. developed SCHNAPPS, the single-cell RNA-seq computer program and helped in the data analysis. D.J.M., J.T.B., and M.P. were all PI members of the MITRAL leducq networks. M.P. supervised the study, performed some experiments, and wrote the manuscript. J.T.B. supervised the study and edited the manuscript. D.J.M. supervised part of the study. **Competing interests:** B.J. is an inventor on a patent application related to this work filed by Pasteur Institute (no. nÂ° IDDN.FR.001.360016.000.S.P.2020.000.31235, filed 9 February 2020). The authors declare that they have no other competing interests. **Data and materials availability:** All data needed to evaluate the conclusions in the paper are present in the paper and/or the Supplementary Materials.

Submitted 19 November 2020
Accepted 17 September 2021
Published 5 November 2021
10.1126/sciadv.abf7910

ScienceAdvances

OCT4-mediated inflammation induces cell reprogramming at the origin of cardiac valve development and calcification

Emily J. Farrar, Emilye Hiriart, Ablajan Mahmut, Bernd Jagla, David S. Peal, David J. Milan, Jonathan T. Butcher, and Michel Puceat

Sci. Adv., **7** (45), eabf7910.
DOI: 10.1126/sciadv.abf7910